ELSEVIER

Materials Science and Engineering A 419 (2006) 196–201

MATERIALS SCIENCE & ENGINEERING A

www.elsevier.com/locate/msea

Optimum definition of true strain beneath a spherical indenter for deriving indentation flow curves

Eun-chae Jeon [a,*], Ju-Young Kim [a], Min-Kyung Baik [a], Sung-Hoon Kim [a], Joo-Seung Park [b], Dongil Kwon [a]

[a] *School of Materials Science and Engineering, Seoul National University, San 56-1, Shillim-dong, Gwanak-gu, Seoul 151-744, South Korea*
[b] *Korea Agency for Technology and Standards, Ministry of Commerce, Industry and Energy, Gwacheon 427-716, South Korea*

Received in revised form 15 December 2005; accepted 15 December 2005

Abstract

Several methods have been suggested for deriving indentation flow curves using the instrumented indentation technique, in which true stress and true strain are defined with indentation parameters. The definition of true stress is nearly the same in all methods, but the definitions of true strain fall into two categories, sine function and tangent function. We adopted the work-hardening exponent to determine the definition appropriate in obtaining accurate indentation flow curves. The work-hardening exponent was proven to be affected only by the definition of true strain and not by other parameters when the effect of real contact depth was eliminated using finite element analysis. The sine function yields too large work-hardening behaviors for materials that obey power-law work-hardening, but the tangent function evaluates them accurately. The definition based on the tangent function was thus determined to be more appropriate in deriving the indentation flow curve.
© 2006 Elsevier B.V. All rights reserved.

Keywords: Instrumented indentation technique; True strain; Indentation flow curve; Work-hardening exponent; Finite element analysis

1. Introduction

The tensile properties of materials, primarily yield strength, tensile strength and work-hardening exponent, are generally considered the most important properties, and the uniaxial tensile test is considered the most reproducible and reliable test. However, its limits on specimen size and the disadvantages of a destructive test method make the uniaxial tensile test inapplicable to micromaterials and materials in service. The instrumented indentation technique was devised to overcome these deficiencies. Since the instrumented indentation technique is nondestructive, can be performed on very limited local areas, and has no restrictions on specimen size and shape, it has a very high potential for extensive in-field use.

Various mechanical properties can be derived from the load–depth curve, which records the continuous variation of indentation depth with load applied by an indenter of specific shape. At an early stage this method yielded only elastic modulus and hardness [1,2]; now, however, it has been extended to produce residual stress [3,4], viscoelasticity [5,6], fracture toughness [7], and indentation tensile properties [8,9]. In addition, methods for evaluating indentation tensile properties have been applied to materials in service [10], and the standards organizations (ISO and ASTM) are developing standards for such tests. However, researchers still are not agreed on the definition of true strain, which is essential in evaluating indentation tensile properties. Though several definitions have been suggested [12,16], the two generally used are based on sine function and tangent function. This study compares the differences and physical meanings of these two definitions and uses the work-hardening exponent to determine an optimum definition.

2. Theoretical analysis

2.1. Derivation of indentation tensile properties

Indentation test methods generally obtain tensile properties using the algorithm in Fig. 1; though the details in each step can differ, the schematic flow is very similar [8,9]. First, an instrumented indentation test is performed with a spherical indenter and produces a load–depth curve. Since this curve does not include the effect of elastic deflection and plastic pile-up for

* Corresponding author. Tel.: +82 2 880 8404; fax: +82 2 886 4847.
E-mail address: purelife@snu.ac.kr (E.-c. Jeon).

0921-5093/$ – see front matter © 2006 Elsevier B.V. All rights reserved.
doi:10.1016/j.msea.2005.12.012

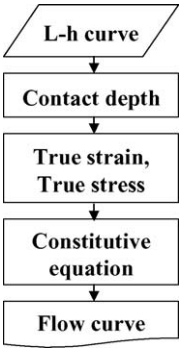

Fig. 1. General algorithm for derivation of indentation flow curve.

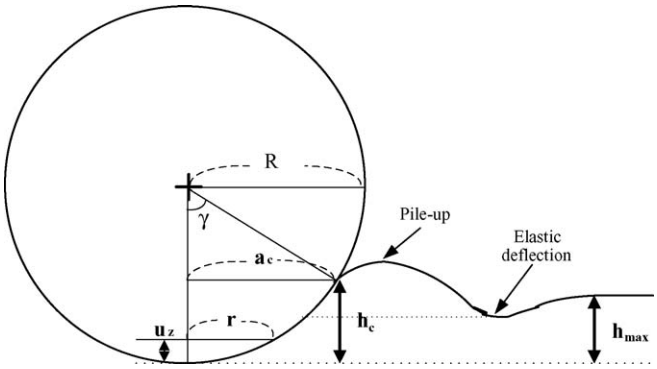

Fig. 2. Schematic diagram of deformation behavior during spherical indentation.

a contact morphology, the indentation depth must be calibrated to the contact depth. Next, the calibrated load–depth curve is used to calculate true stress, a function of contact depth and load, and true strain, a function of contact depth. When these are put into a constitutive equation, a final true stress–true strain curve (indentation flow curve) is drawn.

Different indentation flow curves are obtained from the same load–depth curve if different equations and concepts are used at each step. In particular, the flow curve clearly depends strongly on the definition of true stress and true strain, the two components of the flow curve, and the way in which they are defined is a major factor in whether or not the indentation flow curve agrees with the uniaxial tensile curve.

2.2. Definition of true stress

Materials experience three deformation stages during spherical indentation [11]: in the elastic stage, deformation can be fully recovered if the load is removed; in the elastoplastic stage, plastic deformation occurs under the indenter; finally, in the fully plastic stage, the plastic deformation zone expands to the surface of the material. Since the instrumented indentation technique is usually performed over several hundred N for indentation load and hundreds of μm for indenter radius, the elastic and elastoplastic stages are very difficult to detect. Therefore, in the instrumented indentation technique only the fully plastic stage is considered in calculating the true stress [8].

It is well known that the relationship of true stress (σ) and mean pressure (P_m) can be expressed as [12]:

$$\sigma = \left(\frac{1}{\Psi}\right) P_m = \left(\frac{1}{\Psi}\right)\left(\frac{P}{\pi a_c^2}\right) \quad (1)$$

where Ψ is a plastic constraint factor, P is the load, and a_c is the contact radius between the indenter and the material. Most research on the indentation flow curve has used this definition of true stress. However, the plastic constraint factor has been regarded as a material-independent constant [12] or as a function of the work-hardening exponent [13,14]. In this study, a constant value of 3.0 was used for the plastic constraint factor, as verified by finite element analysis of various materials [15]; this value is also in accord with slip-line field theory [21].

2.3. Definition of true strain

Definitions of true strain are of two kinds, as suggested by Tabor [12] and Ahn and Kwon [8]. After observing residual indentations made by a spherical indenter on various metals, Tabor proposed an experimental definition of true strain using the sine function:

$$\varepsilon = K_1\left(\frac{a_c}{R}\right) = K_1 \sin\gamma \quad (2)$$

where K_1 is generally taken as 0.2, R is the indenter radius, and γ is the half-angle between the indenter and the material; this definition has been widely used in similar work. However, the maximum strain must be constrained under K_1 (generally 0.2) due to the limitation of the sine function, and this makes it difficult to evaluate the indentation flow curves of ductile metals.

On the basis of the deformation shape and strain distribution under a spherical indenter, Ahn and Kwon [8] proposed a new definition using the tangent function. The displacement along the depth axis under the indenter, u_z, can be expressed geometrically as:

$$u_z = h - (R - \sqrt{R^2 - r^2}) \quad (3)$$

here R is the indenter radius and r is a radius at any point on the depth axis (Fig. 2). The shear strain is derived by differentiating the displacement in the depth direction. The maximum shear strain is obtained at $r = a_c$ and Ahn obtained the true strain by using an adjustment constant:

$$\varepsilon = \left(\frac{\alpha}{\sqrt{1-(a_c/R)^2}}\right)\left(\frac{a_c}{R}\right) = \alpha\tan\gamma \quad (4)$$

the adjustment constant was determined as 0.14 independent of material properties by finite element analysis for various materials [15]. This definition covers a large range of true strain, although it also contains the contradiction that maximum strain is infinite when $a_c = R$. However, the experiment is generally finished by the time a_c reaches $0.6R$.

The flow curves should vary according to the definitions of the true strain even when the same load–depth curve is used. Therefore, the definition of true strain must be verified by excluding the parameters within that definition.

2.4. Verification of true strain definition

Two kinds of parameters can affect the indentation flow curve in addition to the definition of true strain. The first is the contact depth, which is essential for calculating true stress and true strain in Eqs. (1), (2) and (4). Because of elastic deflection and pile-up, the contact depth is not same as the depth measured by a displacement sensor, as shown in Fig. 2. It is important to observe the deformation around the loaded indenter while measuring the contact depth. Generally, the elastic deflection can be calibrated by the equation suggested by Oliver and Pharr [2]; the pile-up, however, is very difficult to calibrate and there is no generally accepted equation for doing so. Finite element analysis is widely used to overcome this problem: researchers can measure the contact depth in a loaded state using the deformation morphology produced by a finite element analysis tool [16,17], and thus no calibration equation is needed. Moreover, finite element analysis allows one to vary the mechanical properties at one's convenience, which is very useful in studying the effects of mechanical properties on a certain parameter.

The other parameters that affect the indentation flow curve are the plastic constraint factor in Eq. (1) and the constants in Eqs. (2) and (4). It is very clear that these change the indentation flow curve since they are directly related to true stress and true strain. In this study, the work-hardening exponent was used, which is affected not by them but by the definition of the true strain. The details are discussed in Section 4.3.

3. Finite element analysis

An axisymmetric two-dimensional finite element analysis was performed by a commercial program, ABAQUS finite element code. The specimen mesh was 3738 four-node bilinear axisymmetric elements, as shown in Fig. 3. A fine mesh was set up near the indenter while a coarser mesh was used far from the indenter in order both to reflect the local deformation behavior in the indentation test and to save simulation time. Specimen size was set at 100 mm, large enough to avoid any boundary-induced deformation restrictions. The indenter was assumed perfectly rigid. Other conditions were the same as those in actual experiments [8]. Twenty-five materials, nine real steels (Table 1) and 16 imaginary materials (Table 2), were analyzed. The loading and unloading curves were generated and the contact radius was measured by the ABAQUS postprocessor. From these results, the indentation flow curves were obtained according to the procedure in Fig. 1.

Table 1
Mechanical properties of real materials used in finite element analysis

Materials	Elastic modulus, E (GPa)	Yield strength, YS (MPa)	Work-hardening exponent, n
API X65	204	452	0.154
KP	203	764	0.124
SA508	202	638	0.138
SCM440	207	592	0.160
SCM415	199	290	0.206
SK4	209	336	0.266
STD11	215	243	0.246
STD61	211	349	0.306
SKH51	246	263	0.232

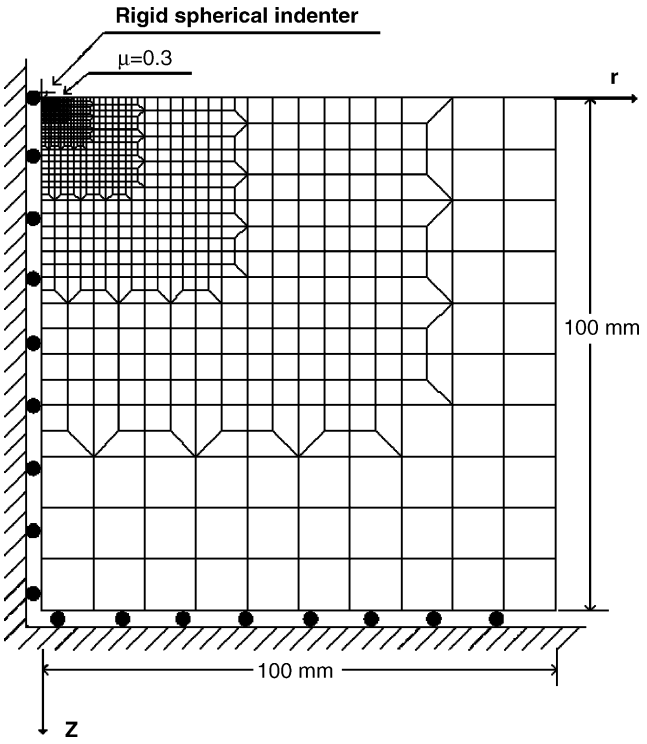

Fig. 3. Mesh and boundary conditions in finite element analysis for spherical indentation. A friction coefficient of 0.3 between indenter and materials was used.

Table 2
Mechanical properties of imaginary materials used in finite element analysis

Elastic modulus, E (GPa)	Yield strength, YS (MPa)	Work-hardening exponent, n
200	200	0.100
200	400	0.100
200	600	0.100
200	800	0.100
200	200	0.200
200	400	0.200
200	600	0.200
200	800	0.200
200	200	0.300
200	400	0.300
200	600	0.300
200	800	0.300
200	400	0.400
200	800	0.400
200	400	0.500
200	800	0.500

4. Results and discussion

4.1. Verification of finite element analysis

Generally, the load–depth curve is a criterion for the applicability of a finite element analysis to an instrumented indentation

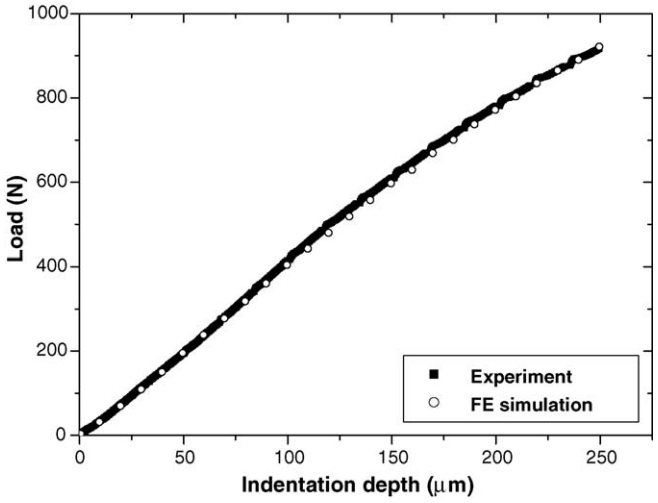

Fig. 4. Comparison of indentation loading curves from an experiment and a finite element analysis (SCM415).

technique. The near-identity of the two load–depth curves in Fig. 4, one obtained from an actual experiment and the other from finite element analysis, suggests that our finite element analysis model was very reasonable and reflected experiments very well. For the nine real steels the two curves were very consistent with one another. In the simulation deformation morphology, pile-up is seen around the indenter. Pile-up occurs in plastic deformation because, since there can be no volume change during deformation, deformed material piles up around the indenter during penetration. Pile-up makes the contact depth greater than the indentation depth measured by a displacement sensor, and is more severe in less work-hardened material [16]. This same phenomenon was observed in our finite element analysis for materials with low work-hardening exponent.

4.2. Derivation of indentation flow curve

The finite element analysis yields the contact depth and the contact radius, which includes the pile-up and elastic deflection. The contact radius was used in calculating true stress (Eq. (1)) and true strain (Eqs. (2) and (4)). Each true stress and true strain was inserted into the constitutive equation (the Hollomon equation [19]):

$$\sigma = K\varepsilon^n \tag{5}$$

where K and n are the strength coefficient and work-hardening exponent, respectively. All the materials used here for finite element analysis obey this equation.

The derived indentation flow curves for SCM415 and one of the ideal materials are presented in Fig. 5. Tabor's indentation flow curves have lower stresses than Ahn's curves below strains of about 0.10 and similar or higher stresses above about 0.10, so that Tabor's curve has a greater slope than Ahn's. Ahn's curves agree with the tensile curves better than Tabor's curve. However, judging which curve is better merely by looking at the graphs may be misleading. We need a quantitative physical criterion that is a variable only of the strain definition and not of K_1 and α in Eqs. (2) and (4), respectively. The work-hardening exponent fits this condition.

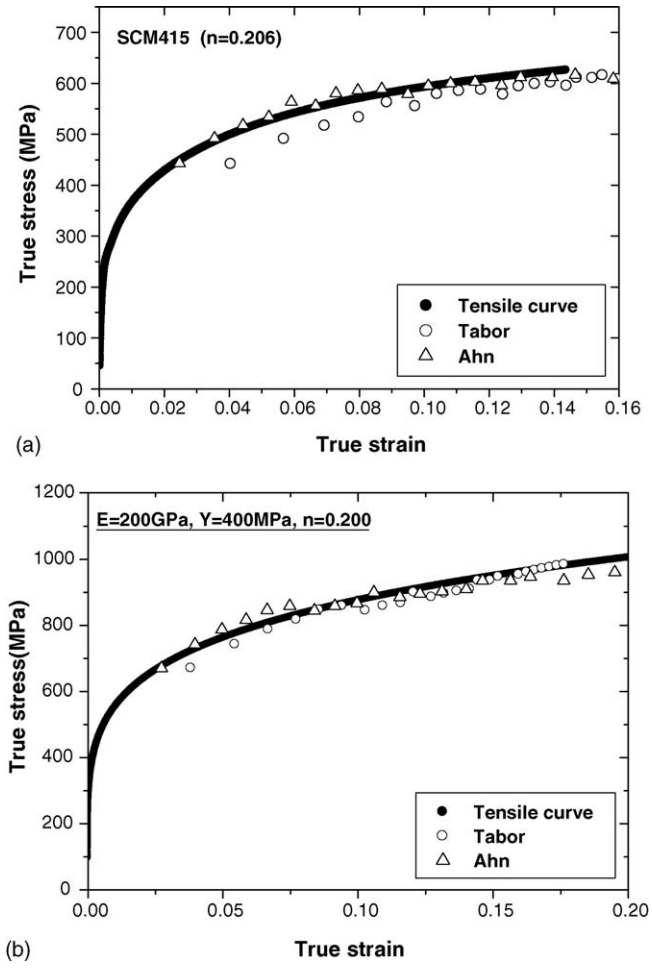

Fig. 5. Comparison of flow curves from tensile tests and finite element analysis for: (a) a real material (SCM415) and (b) an imaginary material (E = 200 GPa, YS = 400 MPa, n = 0.200).

4.3. Derivation of optimum strain definition based on work-hardening exponent

The work-hardening exponent, the exponent in the plastic constitutive equation (Eq. (5)), indicates hardening during plastic deformation; it is well known to be an important factor in the amount of pile-up in spherical indentation [18]. Since the calibration equation for pile-up is expressed by the work-hardening exponent, its exact evaluation is very important in calibrating contact depth. Generally, plastic deformation occurs from the yield strength to the tensile strength in a tensile test. The work-hardening exponent is defined as the slope of Eq. (6), where logarithms are used for the axes of true stress and true strain in this range [20]:

$$\log\sigma = \log K + n\log\varepsilon \tag{6}$$

the same method is used in indentation tests when true stress is obtained from Eq. (1) and true strain from Eqs. (2) or (4). If $k\Psi$ is used in Eq. (1) instead of Ψ (k can be any positive number),

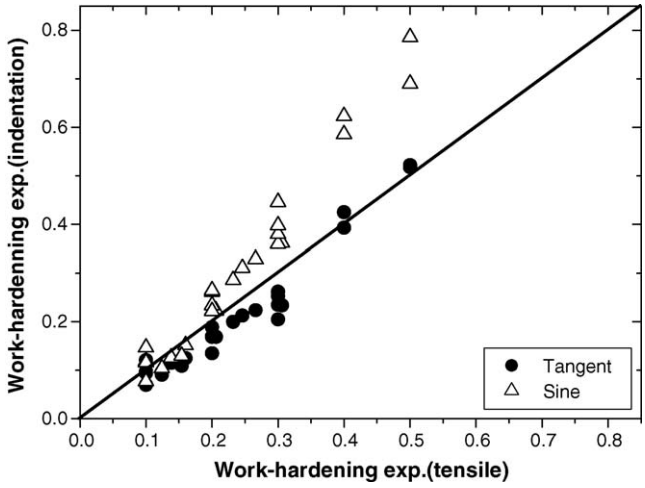

Fig. 6. Work-hardening exponents derived by tangent function and sine function.

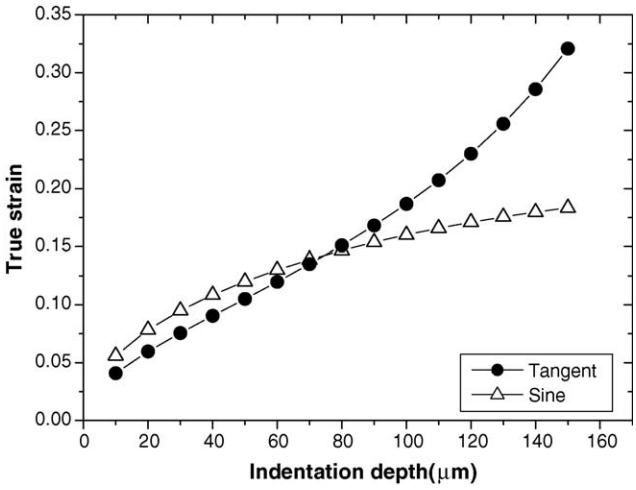

Fig. 7. Variation of strain with indentation depth for tangent function and sine function.

Eq. (6) becomes:

$$\log\sigma = (\log k + \log K) + n\log\varepsilon \tag{7}$$

this equation indicates that the linear curve shifts parallel to the stress axis and the slope does not vary. This means that the work-hardening exponent is constant regardless of the plastic constraint factor. A similar concept can be used for α and K_1 in Eqs. (2) and (4). The constants shift the linear curve parallel to the true strain axis, so that the work-hardening exponent is unchanged. Since this exponent depends only on the functions in the true strain definitions, not on the constants in these definitions, it can be used to determine the appropriate function for the true strain definition.

The work-hardening exponents derived from each strain definition are shown in Fig. 6. The two definitions have similar accuracy below values of 0.2 for the work-hardening exponent: the tangent function underestimates a little and the sine function overestimates a little. However, the sine function overestimates severely above 0.2, while the tangent function produces accurate values. Only the tangent function describes the work-hardening exponent accurately over a large range. Since the work-hardening exponent represents the curvature of the flow curve, its accurate determination is essential in deriving accurate indentation flow curves. Thus the tangent function is more appropriate in predicting the indentation flow curve than the sine function.

This difference can be explained by the behavior of the two functions. In general, they have similar values at low angles, and indeed are often taken as identical there. However, the sine function increases slowly to 1 at high angles while the tangent function goes rapidly to infinity. Fig. 7 presents the true strains calculated by Eqs. (2) and (4) when the indenter radius, α and K_1 are 0.25 mm, 0.14 and 0.2, respectively. Generally, the flow curves of materials that obey Eq. (5) show a slow increase in true stress in the high-strain range. The sine function shows a slow increase in true strain at large depths, which can mean high angle and high true strain. Since the increase in true stress is same for the two definitions, a much greater increase in true stress is observed in the sine function than the tangent function

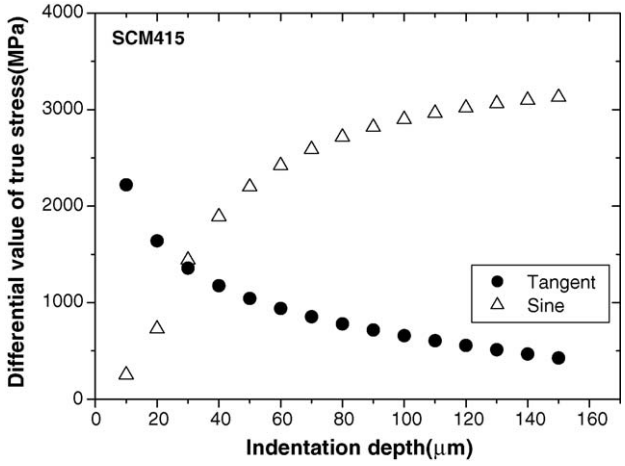

Fig. 8. Comparison of differential values of true stress for tangent function and sine function (SCM415).

at large depths, as seen in Fig. 8. The differential value of the true stress has a similar physical meaning to the work-hardening exponent. The sine function has much larger differential values than the tangent function, and this induces overestimates in the work-hardening exponent. Therefore, the tangent function is the optimum definition for deriving the indentation flow curve of power-law work-hardening materials.

5. Conclusions

Two definitions of true strain have been used in the instrumented indentation technique, one based on a sine function and the other on a tangent function:

$$\varepsilon = K_1\left(\frac{a_c}{R}\right) = K_1\sin\gamma,$$

$$\varepsilon = \left(\frac{\alpha}{\sqrt{1-(a_c/R)^2}}\right)\left(\frac{a_c}{R}\right) = \alpha\tan\gamma$$

The work-hardening exponent was used to evaluate the accuracy of the two definitions. The tangent function evaluates the work-hardening exponent accurately over a large range for materials that obey power-law work-hardening, while the sine function generally overestimates. Therefore, the instrumented indentation technique can produce indentation flow curves as accurate as those produced by a uniaxial tensile test when tangent function is used in the true strain definition.

Acknowledgment

This research was supported by grant 05K1501-01111 from the Center for Nanostructured Materials Technology under the 21st Century Frontier R&D Programs of the Ministry of Science and Technology, Korea.

References

[1] M.F. Doerner, W.D. Nix, J. Mater. Res. 1 (1986) 601.
[2] W.C. Oliver, G.M. Pharr, J. Mater. Res. 7 (1992) 1564.
[3] S. Suresh, A.E. Giannakopoulos, Acta. Mater. 46 (1998) 5755.
[4] Y.H. Lee, D. Kwon, J. Mater. Res. 17 (2002) 901.
[5] S.A.S. Asif, K.J. Wahl, R.J. Colton, Rev. Sci. Inst. 70 (1999) 2408.
[6] D.M. Shinozaki, Y. Lu, J. Elect. Mater. 26 (1997) 852.
[7] J. Malzbender, G. de With, Surf. Techol. 135 (2000) 60.
[8] J.-H. Ahn, D. Kwon, J. Mater. Res. 16 (2001) 3170.
[9] F.M. Haggag, in: W.R. Corwin, F.M. Haggag, W.L. Server (Eds.), Small Specimen Test Techniques Applied to Nuclear Reactor Vessel Thermal Annealing and Plant Life Extension, ASTM STP 1204, 1993, p. 27.
[10] Y. Choi, J.-i. Jang, J. Park, D. Kwon, M. Gao, R. Kania, Oil Gas J. 101 (2003) 66.
[11] H.A. Francis, J. Eng. Mater. Technol. 98 (1976) 272.
[12] D. Tabor, Hardness of Metals, Clarendon Press, Oxford, 1951, p. 2.
[13] B. Taljat, T. Zacharia, F. Kosel, Int. J. Soilds Struct. 35 (1998) 4411.
[14] J.R. Matthews, Acta Metall. 28 (1980) 311.
[15] E.-c. Jeon, M.-K. Baik, S.-H. Kim, B.-W. Lee, D. Kwon, Key Eng. Mater. 297–300 (2005) 2152.
[16] R. Hill, B. Storåkers, A.B. Zdunek, Proc. R. Soc. Lond. A423 (1989) 301.
[17] B. Taljat, T. Zacharia, G.M. Pharr, in: N.R. Moody, W.W. Gerberich, S.P. Baker, N. Burnham (Eds.), Mater. Res. Soc. Symp. Proc., vol. 522, 1998, p. 33.
[18] Y.T. Cheng, C.M. Cheng, Phil. Mag. Lett. 78 (1998) 115.
[19] J.H. Hollomon, Tensile Deformation Trans. AIME 162 (1945) 268.
[20] ASTM E646, Standard test method for tensile strain-hardening exponents (*n*-values) of metallic sheet materials, ASTM International, 2002.
[21] G.E. Dieter, Mechanical Metallurgy, third ed., McGraw Hill, Maidenhead, 1986.